Microsystem Technologies
https://doi.org/10.1007/s00542-024-05803-y

TECHNICAL PAPER

Resiliency improvement through grid forming inverter

Dipanjan Bose[1] · Abhiram Alayil[1] · Sandeep Kumar Chawrasia[1] · Debabrata Roy[1] · Chandan Kumar Chanda[1]

Received: 27 March 2024 / Accepted: 14 October 2024

Abstract
Natural disasters may result in grid outages, which can impact critical loads. Thus, a resilience enhancement-oriented critical load restoration strategy is required. As transmission lines are exposed to these events, critical loads cannot rely on the grid. The microgrid must be able to deliver power to these critical loads during such events. In this scenario, the restoration of critical loads is facilitated by a microgrid, which monitors voltage level disruptions at the point of common coupling (PCC). These disruptions, such as a voltage drop of up to 60%, may occur due to faults or disturbances elsewhere in the network. When the voltage at the PCC drops drastically, an islanding condition arises, during which the inverters should ride through the low voltage (LVRT) condition for up to 0.4 s. A detailed model encompassing both grid-forming and grid-following inverters has been created and simulated using MATLAB. The model accurately replicates the dynamic behavior of active and reactive power supplied to critical loads during grid disturbances. For instance, in the event of a grid fault, the active power delivered to critical loads recovers from 3.26 to 9.05 kW, while reactive power recovers from 1.07 to 2.96 kVAR, ensuring a robust and resilient critical load restoration. The proposed approach is validated by controlling inverters in the microgrid to enhance overall system resilience during disturbances.

1 Introduction

The rapid incorporation of renewable energy sources into the power grid is enhancing the significance of power electronics (Khan et al. 2020; Lin et al. 2020), which presents difficulties for grid operators in maintaining system frequency and rotational inertia. These may cause voltage imbalances as well as frequency imbalances which may lead to a complete blackout (Bose et al. 2020). Therefore the improvement of the resilience (Chanda and Srivastava 2016; Mandal et al. 2021) of the system and restoration of critical loads (Gope et al. 2022) after any operational failure is the biggest challenge. Two inverters are specifically designed for the microgrid. When connected to the grid, Inverter 1 operates in grid-following mode (GFL) and transitions to grid-forming mode (GFM) when operating in islanded mode. Conversely, Inverter 2 is set up to operate in grid-following mode (GFL) whether it is linked to the grid and operating in islanded conditions (D'silva et al. 2023). Inverter 1 is able to sense the islanded condition, and immediately the mode of control is changed from GFL to GFM.

D Bose et al. (Bose et al. 2022) examined the use of blockchain in distributed energy markets, highlighting its ability to facilitate peer-to-peer (P2P) trading without intermediaries, thus reducing transaction costs and increasing efficiency. A case study conducted within this framework demonstrates a tangible improvement in local power system resilience (Bose et al. 2024). This approach highlights the importance of real-time monitoring and adaptive battery operation in ensuring reliable power supply in the face of growing external threats (Ungerland et al. 2023). D. Bose et al. (Bose et al. 2023) partition the grid into manageable sections or voltage control areas to enable more flexible and effective control. A. Selim et at. (Selim et al. 2024) explores the use of grid-forming inverters (GFMs) as a solution for enhancing the stability of low-

✉ Dipanjan Bose
dbose535@gmail.com

Abhiram Alayil
abhiramalayil05@gmail.com

Sandeep Kumar Chawrasia
sandeep.chawrasia9@gmail.com

Debabrata Roy
dbr_roy@yahoo.co.in

Chandan Kumar Chanda
ckc_math@yahoo.com

[1] Department of Electrical Engineering, Indian Institute of Engineering Science and Technology, Shibpur, Howrah, India

Published online: 23 October 2024

inertia distribution systems. F. Sadeque et al. (Sadeque et al. 2024) proposed a novel method that allows inverters to autonomously detect when the utility grid is available for reconnection without relying on external communication.

1.1 Grid connection of inverter

A two-level voltage source inverter has been used here, as the AC side of the voltage source converter provides two levels of outputs $+\frac{V_{DC}}{2}$ and $-\frac{V_{DC}}{2}$. The Voltage Source Converter (VSC) has the ability to transmit power in both directions. The realization of a two-level voltage source inverter can be done by the average modeling of the inverter. Figure 1 depicts the DC-AC half-bridge converter. It consists of two switches, one upper switch (T^+) and one lower switch (T^-). The converter is connected to two ideal voltage sources with a magnitude of $+\frac{V_{DC}}{2}$. The DC midpoint is chosen as the reference node for the measurement of voltage. The AC side of the converter is then linked to the grid via a reactor, which is symbolized by the series RL branch. This reactor will also act as a filter for the AC side of the inverter since it contains harmonics. The power flow direction from the converter to the grid is assumed to be positive.

1.2 Pulse-width modulation

The average output of the AC side of the converter relies upon the duty ratio of the switches. It is mandatory that two switches in a leg should not be in the ON position simultaneously in order to prevent a short circuit of the DC source. Since $f_{sw} \gg f_{grid}$, assuming a constant value, V_{grid} remains unchanged throughout a period of T_{sw}. Here, f_{sw} represents the converter's switching frequency, f_{grid} denotes the fundamental frequency of the grid, and V_{grid} represents the instantaneous value of the grid voltage. From the Fig. 2, the average terminal voltage of VSC is derived as

$$V_{T_{avg}} = m(t)\frac{V_{DC}}{2}; 0 \le m(t) \le 1 \tag{1}$$

where m is the three-phase balanced modulating signal.

Therefore, the average terminal voltage of the VSC in three phases can be written as:

$$\begin{aligned} V_{T_a} &= m_a(t)\frac{V_{DC}}{2} \\ V_{T_b} &= m_b(t)\frac{V_{DC}}{2} \\ V_{T_c} &= m_c(t)\frac{V_{DC}}{2} \end{aligned} \tag{2}$$

2 Power transfer control across two AC systems

The active power flow between two sinusoidal AC sources that have the same fundamental frequencies interconnected with inductance is given by the equation:

$$P = V_{grid} I_{S1} \cos(\theta) = \frac{V_{inv} V_{grid}}{X_S} \sin\delta \tag{3}$$

The reactive power flow is given by the equation

$$Q = V_{grid} I_{S1} \sin(\theta) = \frac{V_{grid}^2}{X_S}\left[1 - \frac{V_{inv}}{V_{grid}}\cos\delta\right] \tag{4}$$

V_{inv} represents the root mean square (RMS) value of the converter output voltage when it operates as an inverter. V_{grid} represents the RMS value of the grid voltage. X_S represents the reactance at the fundamental frequency of the power supply. δ represents the phase difference between the inverter output and the grid voltage phasors, shown in Fig. 3.

The preceding two equations demonstrate that the necessary active power and reactive power flow can be attained by regulating the phase difference and magnitudes of two voltage phasors. From Fig. 3,

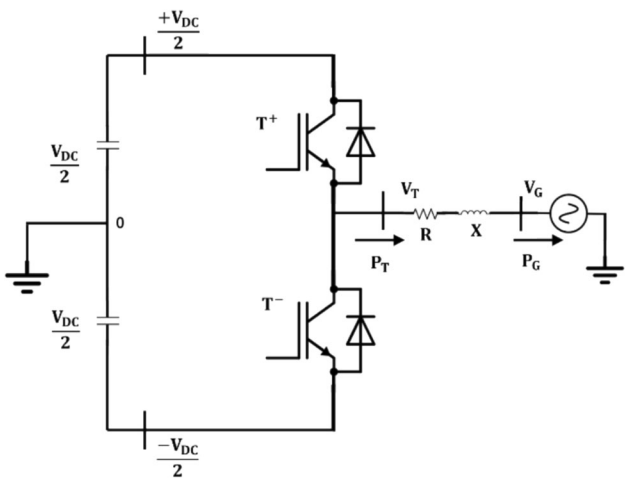

Fig. 1 Average model of the converter

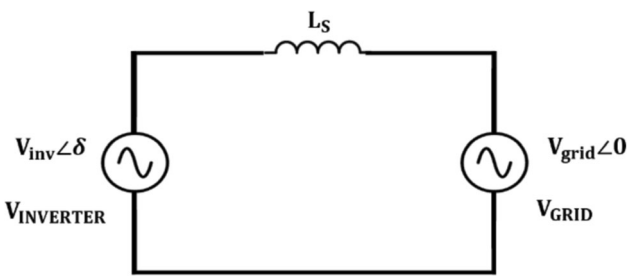

Fig. 2 Inverter interfaced with the grid through reactance

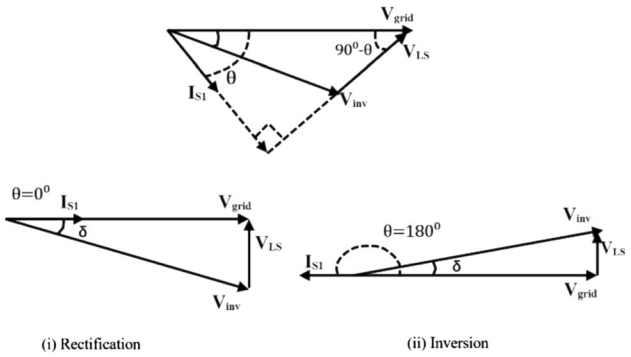

Fig. 3 Phasor diagram showing (i) Rectification and (ii) inversion at UPF

$$V_{grid} = V_{inv} + V_{Ls}$$

and

$$V_{Ls} = j\omega L_s I_1 \tag{5}$$

V_{Ls} represents the voltage decrease across the reactor X_S, while I_1 represents the basic component of the current.

According to Fig. 4, the flow of reactive power is determined by the respective magnitudes of the two voltages, whereas the flow of active power is determined by the relative phase difference between them.

PWM is used to regulate the terminal fundamental voltage of the converter, assuming that the DC bus voltage remains constant. By altering the modulation signal, one may effectively regulate both the active and reactive power, as indicated in (1).

3 Control of converter

The dynamical equations of the AC side of the converter (Harnefors et al. 2021) can be obtained from the average model of the converter, as shown in Fig. 1.

$$V_{T_{avg}} - V_{grid} = L\frac{di}{dt} + Ri \tag{6}$$

From (6), i is the state variable, $V_{T_{avg}}$ is the control variable, and V_{grid} is the disturbance input. Power transferred to the grid is the output which is given by $P_S = V_{grid} * i$. From Eq. (1), control variable $V_{T_{avg}}$ is proportional to the modulating signal. So, the control objective is to regulate i at a desired reference value. Figure 5 represents the closed-loop structure to control the value of i at the reference value.

The error signal e is compensated by the compensator $K(s)$ and provides the control signal u. For simplicity, $V_{T_{avg}}$ is written as V_T and V_{grid} is written as V_g from now onwards. In a balanced three-phase system, (6) can be written as (Fig. 6):

$$\begin{aligned} V_{T(a)} - V_{(a)} &= L\frac{di(a)}{dt} + Ri(a) \\ V_{T(b)} - V_{(b)} &= L\frac{di(b)}{dt} + Ri(b) \\ V_{T(c)} - V_{(c)} &= L\frac{di(c)}{dt} + Ri(c) \end{aligned} \tag{7}$$

From (7), in order to have a closed loop control the instantaneous AC voltage and the current flow need to be monitored. In order to reduce the complexity, control is performed in dq-frame.

In dq-frame,

$$\begin{aligned} P(t) &= \frac{3}{2}\left[v_d(t)i_d(t) + v_q(t)i_q(t)\right] \\ Q(t) &= \frac{3}{2}\left[-v_d(t)i_q(t) + v_q(t)i_d(t)\right] \end{aligned} \tag{8}$$

If $v_q = 0$, active power and reactive power will be directly proportional to i_d and i_q respectively. This allows simpler control for the P/Q control of a three-phase Voltage source converter.

4 Grid following control

In (Rocabert et al. 2012), different types of converter control were discussed. It reveals the detailed analysis of control parameters during the steady state and transient state for the application of microgrids. From (7) and selection of $\rho(t)$ at $(\omega t + \theta_0)$, following equations can be deduced,

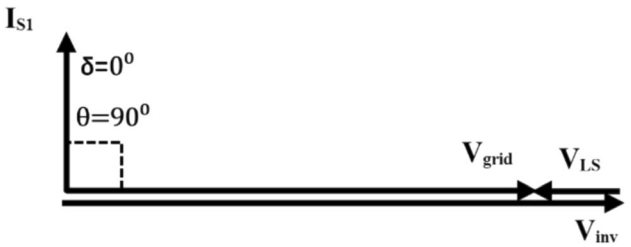

Fig. 4 Phasor diagram of reactive power transfer

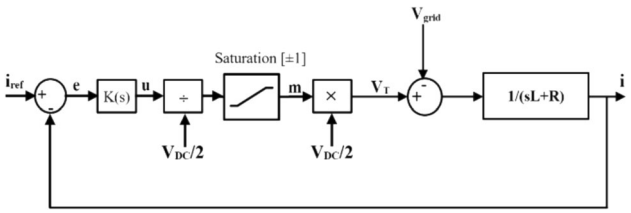

Fig. 5 Closed loop current control of VSC

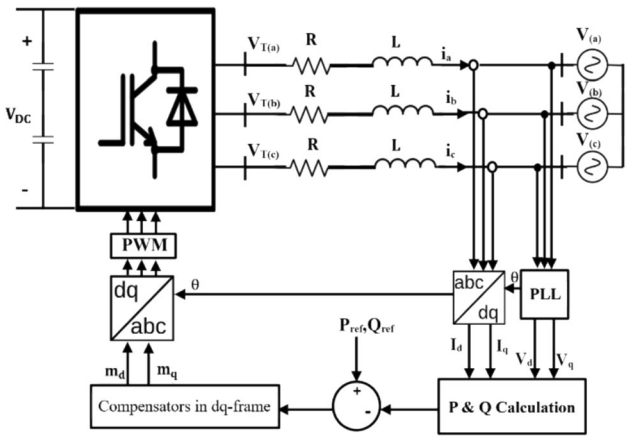

Fig. 6 Current controlled P/Q controller in dq-frame

$$L\frac{di_d}{dt} = L\omega_0(t)i_q - Ri_d + V_{Td} - V_{gd}$$
$$L\frac{di_q}{dt} = -L\omega_0(t)i_d - Ri_q + V_{Tq} - V_{gq} \quad (9)$$

Due to the term $L\omega_0$, i_d and i_q are coupled. It can be decoupled by, determining modulating signals m_d and m_q.

$$m_d(t) = \frac{2}{V_{DC}}\left[u_d - L\omega_0(t)i_q + V_{gd}\right]$$
$$m_q(t) = \frac{2}{V_{DC}}\left[u_q - L\omega_0(t)i_d + V_{gq}\right] \quad (10)$$

where u_d and u_q are two new control inputs. Therefore,

$$V_{td}(t) = \left[u_d - L\omega_0(t)i_q + V_{gd}\right]$$
$$V_{tq}(t) = \left[u_q - L\omega_0(t)i_d + V_{gq}\right] \quad (11)$$

where,

$$u_d = L\frac{di_d}{dt} + Ri_d$$
$$u_q = L\frac{di_q}{dt} + Ri_q \quad (12)$$

A grid-following inverter operates as a current source that runs in parallel with a high impedance, which is subsequently linked to the grid. Therefore, it requires a generator that can create a grid voltage. Any fault or disturbances in the system which may require the isolation of the converter from the grid, results in the maloperation of the inverter. During the islanded condition, if the grid-following converter is supported by another grid-forming converter.

5 Grid forming control

The control of the converter during islanded conditions is depicted in Moubarek Bouzid et al. (2016). Grid forming control is used for maintaining the amplitude and frequency of the load voltage even if some disturbances are present in the load current. Since the VSC is interfaced with the load through an RLC filter which consists of a series RL branch and a shunt capacitor. The capacitance can also provide an impedance to the high-frequency current harmonics.

Dynamic equations of the load voltage are given by the following equations:

$$C\frac{dV_{ga}}{dt} = i_a - i_{La}$$
$$C\frac{dV_{gb}}{dt} = i_b - i_{Lb} \quad (13)$$
$$C\frac{dV_{gc}}{dt} = i_c - i_{Lc}$$

In dq-frame, Eq. (13) can be written as:

$$C\frac{dV_{gd}}{dt} = C\omega_0 V_{gq} + i_d - i_{Ld}$$
$$C\frac{dV_{gq}}{dt} = -C\omega_0 V_{gd} + i_q - i_{Lq} \quad (14)$$

The coupling due to V_{qd} and V_{gq} are decoupled with feed forward compensation, thus V_{gd} and V_{gq} are controlled by $i_{d_{ref}}$ and $i_{q_{ref}}$ respectively. From Eq. (14),

$$u_d = C\frac{dV_{gd}}{dt}$$
$$u_q = C\frac{dV_{gq}}{dt} \quad (15)$$

where u_d and u_q are two new control inputs. Therefore, Eq. (14) can be written as:

$$i_{d_{ref}} = u_d - C\omega V_{gq} + i_{Ld}$$
$$i_{q_{ref}} = u_q - C\omega V_{gd} + i_{Lq} \quad (16)$$

These dq-frame current reference values are now acting as the reference values of the current control loop. The grid-forming inverters operate in a closed loop with desired AC output voltage V^* and frequency f^*. They function as a perfect voltage source connected in series with an impedance.

6 LCL filters in grid-tied inverters

Passive filters play a vital role in ensuring that grid-connected inverters comply with grid rules. The inverter output voltage and current are going to have ripple components

(Kim and Kim 2019). This ripple needs to be attenuated or eliminated. These waveforms need to be nearby sinusoidal. The L filter can attenuate the harmonics but cannot eliminate higher-order harmonics. LC filter will eliminate higher-order harmonics to a further extent. However, the LCL filter is more cost-efficient as it reduces the size of the inductor. However, the design of an LCL filter is far more intricate than that of a L filter (Tang et al. 2015; Liserre et al. 2005; Guzman et al. 2019).

The suggested control of the voltage source converter utilizes the pulse width modulation approach. The harmonics from the VSC need to be within the standards for maintaining the power quality of the grid. LCL filter is a third-order LPF that consists of an LC filter and an L filter. The presence of resonance creates problems that impact both the power quality and the stability of the inverter. The resonant frequency needs to be calculated for designing the LCL filter.

The LCL filter comprises three components. The inverter side inductor was assigned to reducing the amplitude of inverter current harmonics, while the grid side inductor is responsible for mitigating grid side current harmonics. Additionally, a capacitive filter is employed to eliminate higher-order harmonics. The ideal selection of the grid side inductor and inverter side inductor is made. It's a general practice to design the inverter side inductor to be slightly greater than the grid side inductor.

The goal of the filter design is to have an optimal filter inductance ratio, current ripple within acceptable limits, resonance frequency, and reactive power absorbed by the filter.

6.1 LCL filter design

Considering the converter and the grid have symmetrical phase voltages in each phase, the three-phase system can be analyzed as a single-phase system.

Figure 7 describes the LCL filter configuration considering the internal resistance of inductors of the filter in a single-phase system.

$$i_f = \frac{V_I - V_c}{sL_f + R_f}$$

$$i_g = \frac{V_c - V_g}{sL_g + R_g}$$

$$i_c = sC_f V_c$$

$$i_c = i_f - i_g \tag{17}$$

The above equations can be derived from Fig. 7 to create a block diagram for the LCL filter shown in Fig. 8.

The transfer function of the LCL filter can be expressed as the quotient of the grid side current (i_g) and the output voltage of the inverter (V_I). The equation for this transfer function is as follows:

$$G(s)_{LCL} = \frac{i_g(s)}{V_I(s)} \tag{18}$$

Let $\tau_f = L_f/R_f$, and $\tau_g = L_g/R_g$ be the time constants of the inductors from gid side and inverter. If $\tau_f = \tau_g = \tau$, then G_{LCL} is

$$G(s)_{LCL} = \frac{1/r(1-r)L^2C_f}{(s+\frac{1}{\tau})(s^2 + 2\xi\omega_{res}s + \omega_{res}^2)} \tag{19}$$

where,

$$\omega_{res} = \sqrt{\frac{1}{r(1-r)LC_f}} \tag{20}$$

$$\xi = \frac{1}{2\omega_{res}\tau} \tag{21}$$

Here, $L = L_f + L_g$, and $r = L_f/L$.

The selection of the LCL filter parameters is determined by the converter's power rating, switching frequency, and basic grid frequency. The filter impedances must be represented in terms of the base values.

$$G(s)_{LCL} = \frac{\frac{1}{L_f L_g C_f}}{s^3 + \left[\left(\frac{1}{\tau_f} + \frac{1}{\tau_g}\right)\right]s^2 + \left[\left(\frac{1}{\tau_f \tau_g}\right) + \left(\frac{L_f + L_g}{L_f L_g C_f}\right)\right]s + \left[\left(\frac{1}{\tau_f L_g C_f}\right) + \left(\frac{1}{\tau_g L_f C_f}\right)\right]} \tag{22}$$

Figure 9 depicts the design for the LCL filter and bode diagram.

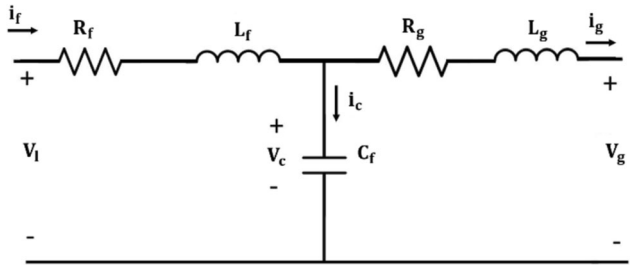

Fig. 7 LCL filter configuration

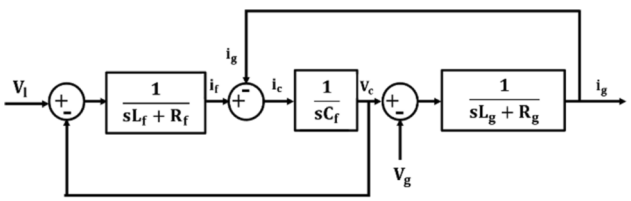

Fig. 8 Block diagram for LCL filter

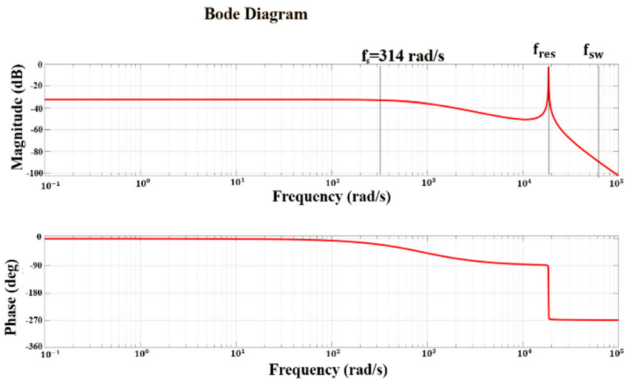

Fig. 9 Bode diagram of $G(s)$

$$Z_b = \frac{(V_n)^2}{P_n} \tag{23}$$

$$C_b = \frac{1}{\omega_n Z_b} \tag{24}$$

V_n represents the nominal rms line voltage, ω_n represents the fundamental grid frequency, and P_n represents the active power rating of the converter. The filter inductance ratio is selected to be 0.6. The overall inductance of the filter can be determined by design as shown below:

$$L > \frac{V_{DC}}{12 f_{sw} \Delta i_{LP} P_{max}} \tag{25}$$

Additionally, it is necessary for the total inductance to be below 0.1 pu in order to minimise the voltage drop across the inductors.

$$2\pi f_g (L_1 + L_2) < 0.1 \frac{v_g^2}{S_{rated}} \tag{26}$$

To avoid excessive consumption of reactive power, the capacitor filter should draw a reactive power that is less than 5% of the rated power.

$$2\pi f_g C V^2 < 0.05 S_{rated} \tag{27}$$

To avoid passive damping, inductance values are chosen such that the resonant frequency lies in the region:

$$\frac{f_s}{6} < f_{res} < \frac{f_s}{2} \tag{28}$$

where f_s is the swiching frequency and f_{res} is the resonant frequency.

Different parameters of the designed LCL filter have been shown in Table 1.

Table 1 Parameters of LCL filter

Sl no	Parameter	Value
1	Power at rated supply	5 kW
2	Voltage at the Grid	400 V
3	Voltage at DC Link	800 V
4	Frequency for Switching	10 kHz
5	Fundamental Frequency at Grid	50 Hz
6	L_f	1.5 mH
7	L_g	1 mH
8	C_f	2 μF

7 Simulations and results

The controllers designed for the operation of microgrids in both grid-connected and islanded modes of operation with the help of synchronization algorithms were tested under various situations. The complete block diagram of the Simulink model is shown in Fig. 10.

The inverters DG_1 and DG_2 were initially not connected to the grid. Let the DG_1 operate as grid forming initially and waited till $t = 0.15$ s for settling the transients. DG_2 is connected to DG_1 only at $t = 0.15$ s to avoid any oscillation problems when grid forming on DG_1. At this instant, DG_2 takes DG_1 as the reference to operate. The circuit breaker is closed only at $t = 0.3$ s, for settling the transients produced by DG_2, and now it is operating in grid-connected mode as depicted in Fig. 11 and 12.

Each inverter has a power rating of 5KW with a tolerance of ± 10% for active power and ± 10% for reactive power in KVAr at the filter output under steady-state conditions. The inverter converts the DC bus voltage to the nominal three-phase AC grid voltage of amplitude 400 V, V_{rms} and fundamental frequency 50 Hz. The inverter is capable of detecting and switching between grid-connected mode and islanded mode.

Figure 13 depicts the electrical current passing through the circuit breaker under normal operating conditions. Figure 14 displays the active and reactive power flow during typical operation.

The local load at the inverter terminals is rated for operating at 10 KW at 0.95 power factor lagging.

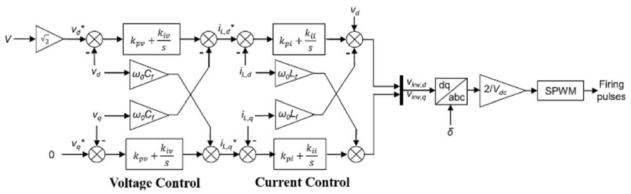

Fig. 10 Complete block diagram of the Simulink model

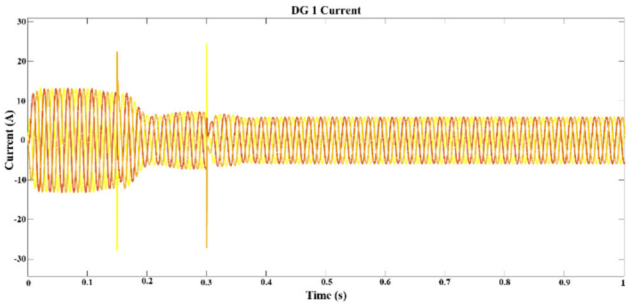

Fig. 11 Output current from DG_1

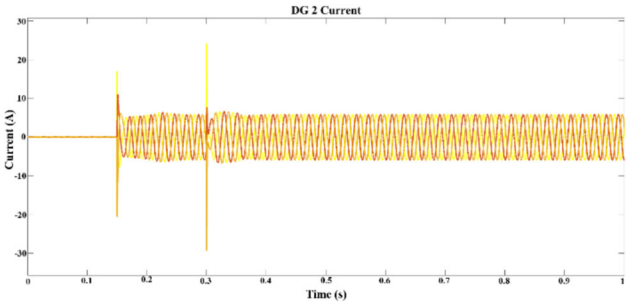

Fig. 12 Output current from DG_2

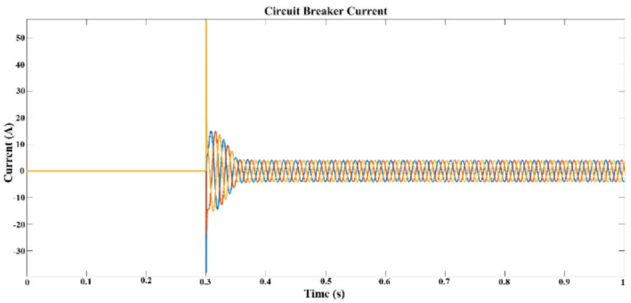

Fig. 13 Current through circuit breaker

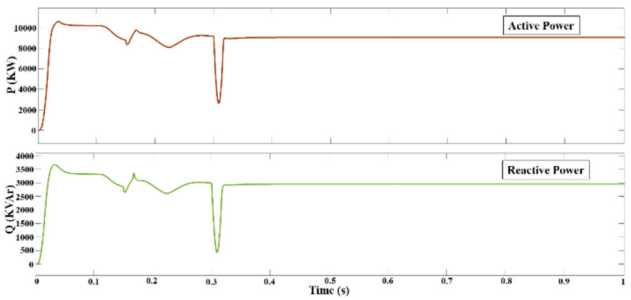

Fig. 14 Active and reactive power drawn by the local load

7.1 Case study

The grid disturbance needs to be simulated for the response of the inverters during the event. At $t = 0.8$ s, a three-phase fault occurs at any part of the network. The high short circuit current result in a large voltage dip as shown in Fig. 15. Eventually, the RMS voltage at PCC was reduced to 60%. As per IEEE 2800, if any fault in the system occurred, DERs should not be tripped immediately. It should have the Low Voltage-Ride Through (LVRT) capability. It should stay connected to the network, providing some voltage support by injecting reactive power at PCC. If the low voltage condition at PCC prevails greater than a certain time, it should then be tripped.

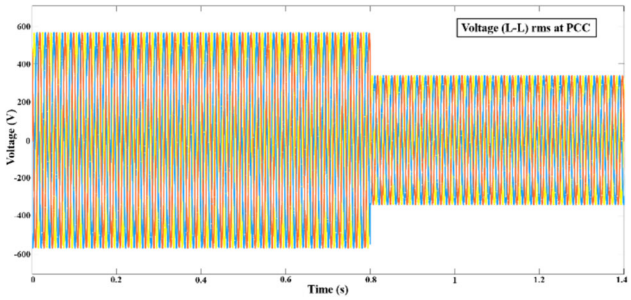

Fig. 15 Three phase Voltage ($V_{LL_{rms}}$) at PCC

The inverters waited for 0.4 s to check whether the voltage level at PCC is improved. At $t = 1.2$ s, CB was open and the inverter turned to islanded mode operation/ grid forming control.

From Fig. 16, it is clear that the voltage dip at PCC causes a huge current to draw from PCC to meet the load demand. The islanding detection is done, and then the inverter turns to grid-forming mode at $t = 1.2$ s.

From Fig. 17, a severe dip in the voltage at PCC causes a huge depression in the power fed to the local critical load. Figure 17 is the graph that plots the active power and reactive power fed to the critical loads during the grid disturbances as a function of time, which is nothing but the resilience curve. It is evident from the figure that the resilience has been improved by the microgrid.

The entire event can be described as follows:

- At $t = 0.15$ s, DG_2 is connected to DG_1.
- At $t = 0.30$ s, the microgrid is in grid-connected mode/ grid following mode.
- At $t = 0.8$ s, a large voltage dip at PCC occurred due to a fault at any other part of the network.

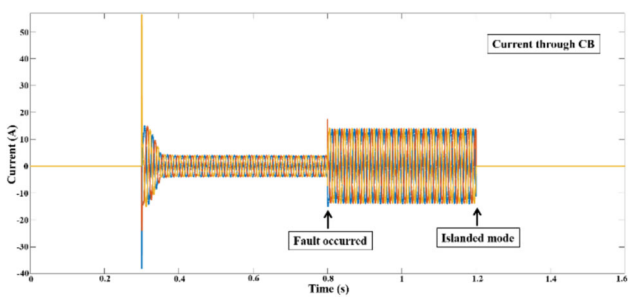

Fig. 16 Current flow through CB during grid disturbance

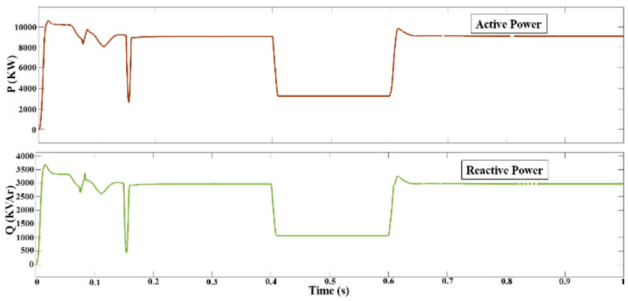

Fig. 17 Active and reactive power drawn by the local load during grid disturbances

- From $t = 0.8$ s to $t = 1.2$ s, the inverter still operated in the grid following mode to check whether the voltage profile at PCC will improve.
- At $t = 1.2$ s, inverter operated in islanded mode/ grid forming mode.

The voltage dip at PCC causes the active power fed to the critical load drastically drops from 9.05 KW to 3.26 KW and the reactive power drop from 2.96 KVAr to 1.07 KVAr. The active power which is not served is thus 5.79 KW and the reactive power not served is 1.89 KVAr.

8 Conclusion

A detailed model of grid-forming and grid-following inverters has been developed using MATLAB to precisely simulate the dynamic response of active and reactive electricity delivered to the essential load during grid disruptions. The model includes a current control loop for following the grid and an inner voltage loop for creating the grid. Both loops are implemented using PI control.

The suggested technique prioritizes the restoration of critical loads in a microgrid by utilizing control over the inverters, with a specific emphasis on resilience. The inverter control was rapidly switched from grid following to grid forming mode, resulting in the restoration of critical load in an impressive timeframe of only 0.4 s. The quick response time guarantees uninterrupted support for critical loads, even during grid outages, hence improving the overall reliability and resilience of the microgrid system.

Moreover, the effectiveness of the suggested control method exhibits its capability for implementation in practical situations, where ensuring continuous power delivery to critical loads is of utmost significance. This research contributes to the advancement of microgrid control and resilience, which in turn leads to the development of more dependable and reliable power systems in response to changing grid problems and uncertainties.

Acknowledgements The authors wanted to extend their appreciation to the Department of Electrical Engineering of the Indian Institute of Engineering Science and Technology, Shibpur, for providing support and a state-of-the-art research facility during the research.

Author contribution Dipanjan Bose developed the research study, while Abhiram Alayil designed the technique, carried out the investigation, and did the formal analysis. Sandeep Kumar Chawrasia and Abhiram Alayil were involved in the process of organising and managing the data, and creating visual representations of the findings. Dipanjan Bose and Abhiram Alayil were responsible for composing the initial document, as well as reviewing, editing, and preparing it for submission. Dr. Debabrata Roy and Dr. Chandan Kumar Chanda oversaw the project, and allocated resources for the research. All authors have reviewed and consented to the final version of the manuscript.

Funding The authors declare that there is no financial involvement or conflict of interest related to this research study.

Data availability No datasets were generated or analysed during the current study.

Declarations

Conflict of interest The authors declare no conflict of interests.

References

Bose D, Chanda CK, Chakrabarti A (2020) Vulnerability assessment of a power transmission network employing complex network theory in a resilience framework. Microsyst Technol 26(8):2443–2451

Bose D, Chanda CK, Chakrabarti A (2022) Blockchain insisted resilience enhancement of power electricity markets using distributed energy trading. Int J Emerg Electr Power Syst 23(5):663–671

Bose D, Sarkar P, Chanda CK, Chakrabarti A (2024) Evaluation of percolation theory insisted resilience index for indian 62 bus utility system in cascading failure situation. J Inst Eng India Ser B. https://doi.org/10.1007/s40031-024-01075-2

Bose D, Mandal M, Paul A, Choudhuri R, Roy D, Chanda CK (2023) Electrical distance based ML-assisted clustering case study on Indian 62-bus utility grid for voltage control area determination. In: 2023 5th International Conference on Energy, Power and Environment: Towards Flexible Green Energy Technologies (ICEPE) (pp. 1–6). IEEE

Chanda S, Srivastava AK (2016) Defining and enabling resiliency of electric distribution systems with multiple microgrids. IEEE Trans Smart Grid 7(6):2859–2868

D'silva S, Zare A, Shadmand MB, Bayhan S, Abu-Rub H (2023.) "Towards resiliency enhancement of network of grid-forming and grid-following inverters," IEEE Transactions on Industrial Electronics, pp. 1–11

Gope S, Dutta I, Roy K, Chakrabarti I, Bose D, Chanda CK (2022) "Crewman deployment model for improving the resiliency of the power system." Int Conf Intell Controll Comput Smart Power (ICICCSP) 2022:1–5

Guzman R, de Vicuna LG, Camacho A, Miret J, Rey JM (2019)˜ "Receding-horizon model-predictive control for a three-phase vsi with an lcl filter." IEEE Trans Industr Electron 66(9):6671–6680

Harnefors L, Kukkola J, Routimo M, Hinkkanen M, Wang X (2021) A universal controller for grid-connected voltage-source converters. IEEE J Emerg Sel Topics in Power Electron 9(5):5761–5770

Khan A, Hosseinzadehtaher M, Shadmand MB, Bayhan S, Abu-Rub H (2020) On the stability of the power electronics-dominated grid: a new energy paradigm. IEEE Ind Electron Mag 14(4):65–78

Kim Y-J, Kim H (2019) Optimal design of lcl filter in grid-connected inverters. IET Power Electron 12(7):1774–1782. https://doi.org/10.1049/ietpel.2018.5518

Lin Y, et.al. (2020) "Research roadmap on grid-forming inverters," National Renewable Energy Lab. (NREL), Golden, CO (United States)

Liserre M, Blaabjerg F, Hansen S (2005) Design and control of an lcl-filter-based three-phase active rectifier. IEEE Trans Ind Appl 41(5):1281–1291

Mandal M, Bose D, Chanda CK (2021) "Voltage profile improvement by using dgs in power system resilient framework," in 2021 IEEE International Conference on Power, Electrical, Electronic and Industrial Applications (PEEIACON), pp. 16–20

El Moubarek Bouzid A, Sicard P, Yamane A, Paquin J.-N (2016)"Simulation of droop control strategy for parallel inverters in autonomous ac microgrids," In: 2016 8th International Conference on Modelling, Identification and Control (ICMIC), pp. 701–706

Rocabert J, Luna A, Blaabjerg F, Rodríguez P (2012) "Control of power converters in ac microgrids," pp. 4734–4749

Sadeque F, Gursoy M, Mirafzal B (2024) Grid-forming inverters in a microgrid: maintaining power during an outage and restoring connection to the utility grid without communication. IEEE Trans Ind Electron. https://doi.org/10.1109/TIE.2024.3349574

Selim A, Zhao J, Seo GS, Ding F, Cui B (2024) Grid-forming inverters for enhancing stability and resilience in distribution networks under transients and restoration. In 2024 IEEE Power & Energy Society Innovative Smart Grid Technologies Conference (ISGT) (pp. 1–5). IEEE

Tang Y, Yao W, Loh PC, Blaabjerg F (2015) "Design of lcl-filters with lcl resonance frequencies beyond the nyquist frequency for grid-connected inverters." IEEE Energy Convers Congr Exposition (ECCE) 2015:5137–5144

Ungerland J, Denninger R, Werner D, Schroven K, Lickert B, Köpke C, Stolz A (2023) Improving power system resilience based on grid-forming converter control and real-time monitoring. In: 2023 8th IEEE Workshop on the Electronic Grid (eGRID) (pp. 1–6). IEEE

Terms and Conditions

Springer Nature journal content, brought to you courtesy of Springer Nature Customer Service Center GmbH (“Springer Nature”).
Springer Nature supports a reasonable amount of sharing of research papers by authors, subscribers and authorised users (“Users”), for small-scale personal, non-commercial use provided that all copyright, trade and service marks and other proprietary notices are maintained. By accessing, sharing, receiving or otherwise using the Springer Nature journal content you agree to these terms of use (“Terms”). For these purposes, Springer Nature considers academic use (by researchers and students) to be non-commercial.
These Terms are supplementary and will apply in addition to any applicable website terms and conditions, a relevant site licence or a personal subscription. These Terms will prevail over any conflict or ambiguity with regards to the relevant terms, a site licence or a personal subscription (to the extent of the conflict or ambiguity only). For Creative Commons-licensed articles, the terms of the Creative Commons license used will apply.
We collect and use personal data to provide access to the Springer Nature journal content. We may also use these personal data internally within ResearchGate and Springer Nature and as agreed share it, in an anonymised way, for purposes of tracking, analysis and reporting. We will not otherwise disclose your personal data outside the ResearchGate or the Springer Nature group of companies unless we have your permission as detailed in the Privacy Policy.
While Users may use the Springer Nature journal content for small scale, personal non-commercial use, it is important to note that Users may not:

1. use such content for the purpose of providing other users with access on a regular or large scale basis or as a means to circumvent access control;
2. use such content where to do so would be considered a criminal or statutory offence in any jurisdiction, or gives rise to civil liability, or is otherwise unlawful;
3. falsely or misleadingly imply or suggest endorsement, approval , sponsorship, or association unless explicitly agreed to by Springer Nature in writing;
4. use bots or other automated methods to access the content or redirect messages
5. override any security feature or exclusionary protocol; or
6. share the content in order to create substitute for Springer Nature products or services or a systematic database of Springer Nature journal content.

In line with the restriction against commercial use, Springer Nature does not permit the creation of a product or service that creates revenue, royalties, rent or income from our content or its inclusion as part of a paid for service or for other commercial gain. Springer Nature journal content cannot be used for inter-library loans and librarians may not upload Springer Nature journal content on a large scale into their, or any other, institutional repository.
These terms of use are reviewed regularly and may be amended at any time. Springer Nature is not obligated to publish any information or content on this website and may remove it or features or functionality at our sole discretion, at any time with or without notice. Springer Nature may revoke this licence to you at any time and remove access to any copies of the Springer Nature journal content which have been saved.
To the fullest extent permitted by law, Springer Nature makes no warranties, representations or guarantees to Users, either express or implied with respect to the Springer nature journal content and all parties disclaim and waive any implied warranties or warranties imposed by law, including merchantability or fitness for any particular purpose.
Please note that these rights do not automatically extend to content, data or other material published by Springer Nature that may be licensed from third parties.
If you would like to use or distribute our Springer Nature journal content to a wider audience or on a regular basis or in any other manner not expressly permitted by these Terms, please contact Springer Nature at

onlineservice@springernature.com